



**QUEEN'S
UNIVERSITY
BELFAST**

Simulating and predicting cellular and in vivo responses of colon cancer to combined treatment with chemotherapy and IAP antagonist Birinapant/TL32711

Crawford, N., Salvucci, M., Hellwig, C. T., Lincoln, F. A., Mooney, R. E., O'Connor, C. L., Prehn, J. HM., Longley, D. B., & Rehm, M. (2018). Simulating and predicting cellular and in vivo responses of colon cancer to combined treatment with chemotherapy and IAP antagonist Birinapant/TL32711. *Cell Death and Differentiation*, 25, 1952. <https://doi.org/10.1038/s41418-018-0082-y>

Published in:
Cell Death and Differentiation

Document Version:
Peer reviewed version

Queen's University Belfast - Research Portal:
[Link to publication record in Queen's University Belfast Research Portal](#)

Publisher rights

© 2018 The Authors.

This work is made available online in accordance with the publisher's policies. Please refer to any applicable terms of use of the publisher.

General rights

Copyright for the publications made accessible via the Queen's University Belfast Research Portal is retained by the author(s) and / or other copyright owners and it is a condition of accessing these publications that users recognise and abide by the legal requirements associated with these rights.

Take down policy

The Research Portal is Queen's institutional repository that provides access to Queen's research output. Every effort has been made to ensure that content in the Research Portal does not infringe any person's rights, or applicable UK laws. If you discover content in the Research Portal that you believe breaches copyright or violates any law, please contact openaccess@qub.ac.uk.

Simulating and predicting cellular and *in vivo* responses of colon cancer to combined treatment with chemotherapy and IAP antagonist Birinapant/TL32711

Running title: Chemotherapy/IAP antagonist responsiveness in CRC

Nyree Crawford¹, Manuela Salvucci^{2,3}, Christian T Hellwig^{4,5}, Frank A Lincoln^{2,3}, Ruth E Mooney^{2,3}, Carla L O'Connor², Jochen HM Prehn^{2,3}, Daniel B Longley^{1,*}, Markus Rehm^{2,3,4,5*}

¹Cell Death & Drug Resistance Group, Centre for Cancer Research & Cell Biology, Queen's University Belfast, Belfast, UK; ²Department of Physiology & Medical Physics, ³Centre for Systems Medicine, Royal College of Surgeons in Ireland, Dublin 2, Ireland; ⁴Institute of Cell Biology and Immunology, ⁵Stuttgart Research Center Systems Biology, University of Stuttgart, D-70569 Stuttgart, Germany. *Shared senior authorship

Corresponding authors:

Prof. Dr. Markus Rehm
Institute of Cell Biology and Immunology
University of Stuttgart
Allmandring 31
70569 Stuttgart
Germany
E-mail: markus.morrison@izi.uni-stuttgart.de

Prof. Daniel B Longley
Cell Death & Drug Resistance Group
Centre for Cancer Research & Cell Biology
Queen's University Belfast
Belfast
UK
E-mail: d.longley@qub.ac.uk

Funding support: The authors kindly acknowledge support for their work by grants from the European Union (FP7 APO-DECIDE) and Science Foundation Ireland/Department for Employment and Learning Northern Ireland Investigator Programme (14/IA/2582; 13/IA/1881). CTH and FAL received support from the Irish Research Council (GOIPD/2013/102; GOIPG/2014/1299). MR receives further support from the German Research Foundation (FOR2036, MO 3226/1-1).

Abstract

Apoptosis resistance contributes to treatment failure in colorectal cancer (CRC). New treatments that reinstate apoptosis competency have potential to improve patient outcome but require predictive biomarkers to target them to responsive patient populations. Inhibitor of apoptosis proteins (IAPs) suppress apoptosis, contributing to drug resistance; IAP antagonists such as TL32711 have therefore been developed. We developed a systems biology approach for predicting response of CRC cells to chemotherapy and TL32711 combinations *in vitro* and *in vivo*. CRC cells responded poorly to TL32711 monotherapy *in vitro*; however, co-treatment with 5-Fluorouracil (5-FU) and oxaliplatin enhanced TL32711-induced apoptosis. Notably, cells from genetically identical populations responded highly heterogeneously, with caspases being activated both upstream and downstream of mitochondrial outer membrane permeabilisation (MOMP). These data, combined with quantities of key apoptosis regulators were sufficient to replicate *in vitro* cell death profiles by mathematical modelling. *In vivo*, apoptosis protein expression was significantly altered, and mathematical modelling for these conditions predicted higher apoptosis resistance that could nevertheless be overcome by combination of chemotherapy and TL32711. Subsequent experimental observations agreed with these predictions, and the observed effects on tumour growth inhibition correlated robustly with apoptosis competency. We therefore obtained insights into intracellular signal transduction kinetics and their population-based heterogeneities for chemotherapy/TL32711 combinations and provide proof-of-concept that mathematical modelling of apoptosis competency can simulate and predict responsiveness *in vivo*. Being able to predict response to IAP antagonist-based treatments on the background of cell-to-cell heterogeneities in the future might assist in improving treatment stratification approaches for these emerging apoptosis-targeting agents.

Key words: Apoptosis, colorectal cancer, chemotherapy, systems biology, IAP, SMAC.

Introduction

Stage III and high risk stage II colon cancer patients receive adjuvant 5-fluorouracil (5-FU)-based chemotherapy often combined with oxaliplatin. However, 5-FU/oxaliplatin treatment in stage III benefits only 15%-20% of patients (1). Moreover, 5-year OS rates are less than 6% for stage IV metastatic CRC (mCRC) patients treated primarily with 5-FU-based regimens. Current targeted treatments such as anti-EGFR therapies are approved in the metastatic setting only for a subset of patients (*RAS*, *BRAF* wild-type) and are ineffective in the adjuvant setting (2,3). Since pre-existing or acquired resistance to apoptosis significantly contributes to treatment failure in cancer (4), the evaluation of new treatment combinations which reinstate apoptosis competency has the potential to improve patient outcome.

Novel targeted drugs which neutralize apoptosis-inhibiting proteins have potential as enhancers of chemotherapy responsiveness in cancer. The group of intracellular anti-apoptotic proteins is relatively small, with caspase-8/-10 inhibitor FLIP, anti-apoptotic Bcl-2 family members and inhibitor of apoptosis (IAP) proteins being the major players. The Bcl-2 antagonist venetoclax/ABT-199 has recently been approved for the treatment of patients with 17p deleted chronic lymphocytic leukemia and is currently being tested in additional cancers (5). From the group of IAP antagonists that have been evaluated, clinical studies have shown that TL32711/Birinapant (Tetralogics) and LCL161 (Novartis) can be combined safely with a range of chemotherapeutic agents, and both have entered phase 2 trials (<http://clinicaltrials.gov/>) (6). TL32711 generated responses in combination with irinotecan in a subset of colorectal cancer patients who were refractory to irinotecan alone (7). Such response heterogeneities indicate that stratification tools and response predictors will be required to preselect patients likely to respond to IAP antagonist-based combination treatments.

IAP antagonists were initially designed to replicate the function of second mitochondria-derived activator of caspases (SMAC) in binding to and blocking X-linked inhibitor of apoptosis protein (XIAP), the major antagonist of proteases essential for efficient apoptosis execution (caspases-9, -3 and -7) (8). IAP antagonists also bind to and trigger the rapid degradation of cellular IAP (cIAP) 1 and 2 (9), both of which are critical regulators of ripoptosome formation and caspase-8-dependent apoptosis induction in response to intrinsic pro-apoptotic stress and activation of tumour necrosis factor receptor (TNFR) family (6,8). Correspondingly, IAPs have been implicated as mediators of drug resistance in various cancers, including colorectal cancer (10,11).

In this study, we obtained a single cell understanding of signal transduction kinetics and heterogeneities for treatments based on combinations of 5-FU/oxaliplatin and TL32711, and applied a systems biology strategy towards predicting the resulting cell death patterns in populations of colon cancer cells *in vitro* and *in vivo*.

Results

IAP antagonist TL32711/Birinapant sensitizes CRC cell lines to chemotherapy-induced cell death.

XIAP is implicated as an important mediator of clinical drug resistance (12). We assessed the role of XIAP in regulating the apoptotic response of colon cancer cells to the widely used therapeutic combination of 5-FU and oxaliplatin. Genetic loss of XIAP sensitized HCT116 cells to cell death induced by 5-FU/oxaliplatin after 48h of treatment (**Fig.1A**). The cell death induced by 5-FU/oxaliplatin was caspase-dependent (implying apoptosis) since the pan-caspase inhibitor zVAD-fmk abolished cell death in both parental and XIAP null cells (**Fig.1B**). These results indicate that XIAP is an important mediator of resistance to 5-FU/oxaliplatin. We therefore co-treated HCT116 cells with 5-FU and oxaliplatin alone and in combination in the presence or absence of the IAP antagonist TL32711 and determined cell death by flow cytometry. In agreement with results in XIAP null cells, cell death was significantly increased by addition of TL32711 (**Fig.1C**). Similar results were obtained in the LoVo colon cancer model, with TL32711 enhancing apoptosis induced by 5-FU, oxaliplatin and the combination treatment (**Fig.1D**). In both cell lines, TL32711 alone had a relatively modest effect on cell death (~ 10% above background levels).

IAP antagonist TL32711 promotes cIAP1 and cIAP2 depletion, formation of complex II and caspase-8/RIPK1-dependent cell death.

We next further characterised the consequences of and the molecular signalling events initiated by TL32711 treatment. In both HCT116 and LoVo cells, TL32711 caused the rapid and persistent down-regulation of cIAP1 (**Fig.2A**). In many cell lines, cIAP2 expression recovers after initial rapid degradation induced by IAP antagonists; this is because cIAP1 acts as an E3 ligase for cIAP2, and degradation of cIAP1/2 leads to activation of the non-canonical NFκB pathway resulting in increased expression of NFκB-driven genes, including

BIRC3, the gene encoding cIAP2 (13,14). It was therefore notable that cIAP2 expression was also persistently down-regulated in both cell line models in response to TL32711. While it is known that TL32711 also inhibits XIAP ($K_d=45$ nM) (15), the most potent caspase-inhibiting IAP that directly targets caspases-3, -7 and -9, XIAP expression was relatively unaffected by TL32711 in both cell lines (**Fig.2A**); this is consistent with the predominant effect of IAP antagonists on XIAP being disruption of its protein-protein interactions with caspases. In further dose-effect studies, we found that nanomolar concentrations of TL32711 were sufficient to cause the degradation of cIAP1 and cIAP2 in both cell lines (**Fig.2B**).

The loss of cIAPs is known to promote the interaction of procaspase-8 with RIPK1, triggering the formation of complex II or the ripoptosome, a cytosolic caspase-8 activation platform that can trigger apoptosis. Genotoxic stress may also promote ripoptosome formation (16). Assessment of ripoptosome formation indicated that treatment with TL32711 in combination with 5-FU increased RIPK1/procaspase-8 complex formation compared to treatment with TL32711 alone, and this was further enhanced when TL32711 was combined with 5-FU/oxaliplatin (**Fig.2C**), suggesting that standard-of-care chemotherapy promotes ripoptosome formation in colon cancer cells in the context of IAP antagonist treatment (**Fig.2C**). Importantly, this interaction was not observed when cells were exposed only to the chemotherapeutics (**Fig.2C**), indicating that TL32711 initiates an additional pro-apoptotic signalling cascade in parallel to other genotoxic responses in these cells.

Next, we investigated whether the formation of procaspase-8/RIPK1 complexes also results in the activation of caspase-8. To specifically determine initiator caspase-8 activity inside living HCT116 cells, we measured the cleavage of an exogenously expressed CFP-YFP fusion protein containing the preferred caspase-8 cleavage motif IETD by FRET flow cytometry (17,18). To avoid contributions of downstream effector caspases-3 and -7, which both also cleave after IETD motifs, we conducted these experiments in HCT116 cells deficient in Bax and Bak (19). As shown in **Fig.2D**, only treatments including TL32711 resulted in IETD probe cleavage in HCT116 cells. Furthermore, IETDase activity was completely eliminated when these cells were transfected with an siRNA targeting procaspase-8 (**Fig.2D**). We next determined whether caspase-8 activation would be required to trigger MOMP. Indeed, depletion of procaspase-8 expression abolished mitochondrial depolarisation in parental HCT116 cells, specifically in response to TL32711/chemotherapy combination treatments (**Fig.2E**). To complement these analyses, we also depleted RIPK1 expression by

siRNA and determined cell death by flow cytometry; notably, loss of RIPK1 expression also significantly reduced cell death in TL32711 combination treatments (**Fig.2F**).

Taken together, these findings demonstrate that the presence of TL32711 promotes the formation of complexes, presumably ripoptosomes, containing caspase-8 and RIPK1, resulting in upstream caspase-8 activation in a significant proportion of cells. In agreement with this, cell death co-depends on the presence of both procaspase-8 and RIPK1.

Single-cell real-time imaging identifies two distinct caspase activation patterns leading to apoptosis execution in TL32711-based combination treatments.

Next, we analysed the kinetics of intracellular apoptosis signal transduction in HCT116 and LoVo cells that responded to 5-FU/oxaliplatin and TL32711, alone or in combination. To this end, we expressed another CFP-YFP FRET probe, containing a DEVD linker motif preferentially cleaved by caspases-3/-7, but also cleavable by caspase-8 in HCT116 and LoVo cells (20). Readings obtained from this probe (cleavage amounts and kinetics) are also suitable to validate predictions made by deterministic mathematical modelling of apoptosis signalling as to whether apoptosis can be executed efficiently in human cancer cells, including CRC cell lines (21,22). Data obtained from these time-lapse imaging studies, in combination with the results from the previous experimental characterisations, also provided a basis for the subsequent development of an extended mathematical framework for simulating the responsiveness of colon cancer cell populations to treatment combinations that include the IAP antagonist TL32711.

Cells stably expressing the FRET probe were treated and monitored over time by fluorescence microscopy, followed by ratiometric analysis of probe cleavage. As expected, individual cells responded with probe cleavage at different times after treatment (**Fig.3A**). In parallel, cells were loaded with TMRM to obtain data on mitochondrial transmembrane potentials, which depolarise upon MOMP and release of cytochrome c and can serve as a surrogate marker for timing the beginning of the apoptosis execution phase (21,23). For individual cells, fluorescence signals were extracted and plotted to obtain quantitative data on probe cleavage kinetics.

In our measurements, we could observe two prominent response patterns of FRET probe cleavage in single cells (**Fig.3B**). In HCT116 cells, treatment with the chemotherapy combination of 5-FU/oxaliplatin resulted in classical post-MOMP patterns of FRET probe

cleavage during apoptosis execution (**Fig.3Bi**). Only a few cells responded to TL32711, and these presented with an initial phase of slow, modest probe cleavage (**Fig.3Bii**). This “ramp” of substrate cleavage was followed by a transition towards rapid probe cleavage once the execution phase was triggered (**Fig.3Bii**). These patterns were reminiscent of cleavage kinetics previously described by us and others for caspase-8-dependent apoptosis initiation (17,24). Upon combination of chemotherapeutics with TL32711, these dual-phase cleavage patterns were also observed (**Fig.3Biii**) and became more frequent. Nevertheless, a fraction of cells also responded with patterns comparable to chemotherapy-only treatments. Control cells which remained untreated did not display probe cleavage or significant changes in the FRET signal, excluding the possibility that phototoxicity or probe bleaching contributed to the signals recorded (not shown). Similar findings were also made in LoVo cells (**Fig.3Bi-iii**)

An overall quantification of all responses is shown in **Fig.3C,D**. In particular, we determined the onset time of probe cleavage ramps as well as the slope of these ramps, serving as an indicator for pre-MOMP caspase-8 activity. In addition, we determined the mitochondrial MOMP threshold (amount of substrate cleaved at MOMP) as well as the onset time of the post-MOMP execution phase (**Fig.3C,D**). Overall, this demonstrated that moderate probe cleavage (“pre-MOMP ramp”), most likely due to caspase-8 activation (see **Fig.2**), in HCT116 can primarily be observed in the presence of TL32711 (**Fig.3Ci**). In the LoVo model, cells with pre-MOMP substrate cleavage could also be found in response to 5-FU/oxaliplatin, and the fraction of these cells increased when TL32711 was combined with 5-FU/oxaliplatin (**Fig.3Di**). We therefore conclude that response patterns within colon cancer cell populations are heterogeneous, with cells either displaying rapid FRET probe cleavage as expected for apoptosis execution, or initial moderate pre-MOMP caspase-8 activity, which subsequently is converted into rapid apoptosis execution.

Mathematical simulations of apoptosis signalling can recapitulate death profiles and apoptosis sensitization by IAP antagonist TL32711.

Next, we established a mathematical modelling framework that can replicate the apoptosis heterogeneity observed in HCT116 and LoVo cell populations. To this end, we extended a previous deterministic ODE-based model of the apoptosis execution phase that captures the interplay of the apoptosome (cytochrome c-induced APAF-1 oligomerisation and caspase-9 activation), SMAC, XIAP and caspase-3 (21). The terminal outputs of this model are

simulated cleavage kinetics for DEVD caspase substrates, allowing the comparison of model outputs to time-lapse imaging data. Furthermore, we previously showed that >25% substrate cleavage during apoptosis execution is highly indicative of irreversible cell death induction (21). For the model extension here, we included a function which replicates pre-MOMP caspase-8 activity and also implemented a threshold mechanism by which prolonged caspase-8 activity triggers apoptosis execution (see **Fig.4A** and methods). Importantly, we developed this model so that it can capture the cell-to-cell heterogeneity observed experimentally in HCT116 and LoVo cell populations. This was achieved by parameterising *in silico* ensembles of 1,000 cells for each treatment condition, where for each individual cell the respective initial model parameters were sampled from the distributions of experimental input data. To parameterise the reactant amounts, we determined the nM protein expression of key apoptosis regulators in HCT116 and LoVo cells by quantitative Western blotting (12-bit dynamic range) (**Fig.4B**). For the model, these quantities were converted to normal distributions around the measured mean (**Fig.4C**). Similarly, pre-MOMP signalling was parameterised with the experimentally determined heterogeneity data, including the frequency of upstream caspase-8 activation, onset times, activities and MOMP thresholds (see results in **Figs.2, 3**).

In the subsequent simulations for HCT116 cell populations, we noted that chemotherapy or TL32711 on their own induced apoptosis execution in rather few cells of the simulated ensembles (**Fig.4D**). Calculating substrate cleavage and apoptosis execution for the combination of chemotherapy and TL32711 instead showed, as expected, that significantly more cells responded (**Fig.4D**). Similar simulation results were obtained for LoVo cells, with the combination of chemotherapy and TL32711 again resulting in significantly enhanced apoptosis execution (**Fig.4E**). These results therefore demonstrate that mathematical modelling can recapitulate apoptosis responses, the sensitizing effects of TL32711 and cell-to-cell response heterogeneities observed experimentally in populations of colon cancer cells.

Mathematical modelling predicts increased apoptosis resistance of xenografted HCT116 and LoVo cell tumours, which can be overcome by chemotherapy/TL32711 co-treatment.

Next, we assessed whether our mathematical modelling approach would allow us to calculate *in vivo* apoptosis sensitivity and effects on tumour growth in response 5-FU/oxaliplatin and TL32711. To this end, we established xenograft tumour growth models for HCT116 and LoVo cells. Since protein expression amounts in HCT116 and LoVo cells may differ between

in vitro and *in vivo* growth conditions, we first collected tumours grown in untreated control mice for protein quantification. Interestingly, we noted significant differences in apoptosis protein expression amounts between the two growth conditions in both HCT116 and LoVo cells (**Fig.5A-C**). In HCT116 cells, notable decreases in SMAC (1.7-fold), APAF-1 (4.7-fold) and Procaspase-9 (2.1-fold) expression were detected, whereas XIAP expression increased (3.4-fold) (**Fig.5A-C**). We made similar findings in tumours grown from LoVo cells, where again decreases in APAF-1 (3.8-fold) and procaspase-9 (2.7-fold) expression and increases in XIAP (2.1-fold) expression were observed, while procaspase-3 expression also decreased (1.7-fold) in these tumours (**Fig.5A-C**). We therefore used the *in vivo* protein expression data to re-parameterise our model and to calculate whether apoptosis responsiveness of HCT116 and LoVo cell ensembles would be affected. Results from these simulations suggested that for *in vivo* conditions, poor responsiveness to both chemotherapy and TL32711 would be expected, indicating that the changes in protein expression observed in xenograft tumours impair apoptosis execution in a significant fraction of the populations (**Fig.5D,E**, compare to **Fig.4D,E**). The expected *in vivo* heterogeneity in execution efficacy is more explicitly shown in Supplemental Figure 1 (**Fig.S1**). Despite the strong trend towards higher apoptosis resistance, the simulation results also show that the combination of chemotherapy plus TL32711 would notably enhance cell death responses in HCT116 and LoVo xenografts (**Fig.5D,E; Fig.S1**).

Mathematical modelling captures drug effects observed in vivo and predicts treatment responses.

Cell death events accumulated from the cell ensemble simulations (**Fig.5D,E**) indicated that under *in vivo* conditions, the response of HCT116 and LoVo xenografts to chemotherapy and TL32711 combinations is considerably higher than for single treatment (**Fig.6A,B**). To validate the model predictions, we next treated mice growing HCT116 and LoVo cell tumours with 5-FU/oxaliplatin, TL32711 or the combination of both. As mathematically predicted for the *in vivo* setting, for both cell line models we indeed found significantly improved responses upon subjecting mice to the combination treatment with 5-FU/oxaliplatin and TL32711 compared to either 5-FU/oxaliplatin or TL32711 alone (**Fig.6C**). cIAP1 expression was lost and cIAP2 expression decreased in tumour samples following TL32711-based treatments, confirming that the IAP antagonist was efficacious *in vivo*. (**Fig.6D**). Interestingly, we found that cIAP2 expression was downregulated in both xenograft models

following 5-FU/oxaliplatin treatment; however, co-treatment with TL32711 partially restored cIAP2 levels, potentially due to activation of non-canonical NF κ B signalling following TL32711 treatment (8). Most notably, expression of XIAP was reduced in both xenograft models following co-treatment with 5-FU/oxaliplatin and TL32711 (**Fig.6D**).

Next, we examined how well the effects of the different treatments on reducing *in vivo* tumour growth would correlate with the treatment-specific predictions obtained from the mathematical model. We first determined the effects of the different treatments on tumour volume changes over time. To this end, we replicated experimentally measured tumour volume changes of individual mice by a growth impairment model, incorporating factors that represented maximal asymptotic growth and proliferation rates. From this, we obtained the respective drug effects (K_D) that contribute to the observed growth impairment (25,26) (see also methods). The tumour volume changes could be fitted by the growth model, as seen by comparing pooled fitting data on volume changes to experimental data (**Fig.6E,F; Fig.6C**). When plotting cell death predictions against the drug effects obtained from the experimentally observed tumour volume changes (**Fig.6G**), we found that the model predictions indeed correlated strongly with the observed *in vivo* treatment responses. These results therefore confirmed that our mathematical model can predict *in vivo* responses of different CRC cell lines to standard of care chemotherapy, IAP antagonist TL32711 and the combination of both.

Discussion

Colorectal cancer is the 2nd leading cause of cancer-related death in the Western world. In stage IV metastatic disease, median overall survival (OS) is only 21-24 months, 5 year OS rates are <6% and 10 year OS rates <1% (27). IAP antagonists have been demonstrated to synergise with numerous anti-cancer drugs in various model systems (6), and several IAP antagonists are currently in phase II clinical trials (<http://clinicaltrials.gov/>). TL32711 is in clinical trials for the treatment of several advanced solid tumours, haematological malignancies and chronic hepatitis B and has been combined with the apoptosis-inducing human monoclonal antibody conatumumab in patients with relapsed epithelial ovarian cancer (NCT01940172). In a phase II clinical trial combining TL32711 and irinotecan in colorectal cancer patients refractory to irinotecan, the combination was tolerated similar to irinotecan

alone resulted in clinical benefits particularly in patients with mutated *KRAS* (NCT01188499). However, patient selection strategies for IAP antagonists both as monotherapies and in combination with other agents are currently lacking.

Having found that XIAP impairs chemotherapy-induced cell death in CRC cells, we mechanistically and quantitatively characterised the impact of the IAP antagonist TL32711 on chemotherapy-induced cell death *in vitro* and *in vivo*, taking into account cell-to-cell heterogeneity in isogenic cell populations. Subsequently, we developed a systems biology-based approach towards predicting treatment responsiveness to single and combination treatments of TL32711 with standard-of-care CRC chemotherapy in such cell populations. Results from the mathematical simulations correlated robustly with the observed drug effects on xenograft tumour growth in mice.

IAP antagonist-dependent degradation of cIAPs can induce intrinsic ripoptosome formation (30,31), a finding we could confirm in CRC cells treated with TL32711. Interestingly, in contrast to work in fibrosarcoma, breast adenocarcinoma, rhabdomyosarcoma or ovarian carcinoma cell lines (16), chemotherapy alone was not sufficient to induce ripoptosome formation in CRC cells, but significantly enhanced the limited ripoptosome formation observed after TL32711 monotherapy. Consequently, depletion of procaspase-8 or RIPK1 abrogated cell death induced by TL32711/chemotherapy combinations. Our imaging data reveal that in response to TL32711/chemotherapy co-treatment, genetically identical cells differ in their mode of cell death induction, with both pre-MOMP caspase activation being observed (most likely due to ripoptosome formation), as well as subpopulations which trigger MOMP without prior caspase activation. We currently cannot answer where these response heterogeneities emerge from, but speculate that stochastic cell-to-cell heterogeneities in baseline protein expression might be sufficient for these differences. In addition, cell cycle asynchronies might contribute, since a number of apoptosis-regulating proteins are known to be cell cycle regulated and since cells in different phases of the cell cycle will encounter different cell cycle checkpoints upon chemotherapy-induced DNA damage (32). The existing uncertainties regarding these crucial upstream signalling processes as well as the currently limited quantitative and kinetic knowledge of ripoptosome formation are the reasons why in our mathematical model, the upstream signalling was modelled from the behaviour of cell populations.

Of note, it has been reported that certain cell lines might secrete TNF- α and die by autocrine TNFR1-dependent complex II formation and caspase-8 activation. In our studies, neither HCT116 nor LoVo cells secreted TNF- α in response to TL32711 (not shown). However, we cannot exclude that the presence of TNF- α in tumour microenvironments further contributes to treatment efficacy. Indirect evidence for this might emerge in the field of melanoma therapies, where it was recently described that the combination of TL32711 and chemotherapy does not induce response synergies *in vitro*, although single-treatment with TL32711 significantly impaired *in vivo* xenograft growth (33,34). While our systems model already captures *in vivo* drug effects with very promising accuracy for single and combination treatments of TL32711 and CRC chemotherapy, the future inclusion of microenvironmental TNF- α signalling might further improve the performance.

We believe that our approach of using mathematical simulations to predict *in vivo* efficacy of novel apoptosis-targeted agents such as IAP antagonists might have potential for contributing to the future personalisation and optimisation of treatments. We recently demonstrated the added value of mathematically modelling apoptosis competency in combination with clinic-pathological markers for prognosticating disease outcome in chemotherapy-treated stage III CRC patients (35); in the future, similar approaches could be followed for chemotherapy/IAP antagonist combination therapies. Moreover, this basic framework could be extended to take account of the influence of tumour architectures, vascularisation, microenvironmental heterogeneities as well as whole body drug PK/PD (36,37). More advanced experimental models, such as patient-derived xenografts, would provide ideal testing grounds for such model extension, refinement and optimisation.

In summary, this work provides proof-of-principle and in the future could possibly provide the basis for contributing to development of clinical tests in identifying colorectal cancer patients who are most likely to benefit from the addition of IAP antagonists to standard-of-care chemotherapeutics.

Materials and Methods

Compounds and plasmids

TL32711 was obtained from Active Biochem (Maplewood, NJ). 5-FU (Medac) and oxaliplatin (Accord) were obtained from Belfast City Hospital. z-VAD-fmk was purchased from Merck Millipore (Darmstadt, Germany). Plasmids for the expression of the CFP-YFP FRET probes were described previously (17,20).

Cell lines

HCT116 and LoVo cell lines were purchased as authenticated stocks from ATCC (Teddington, UK). HCT116 XIAP⁻⁰ cells were provided by Dr B. Vogelstein (Johns Hopkins University). HCT116 (Bax/Bak)^{-/-} cells were kindly provided by Dr R.J. Youle (National Institute of Neurological Disorders and Stroke).

siRNA Transfections

Scrambled control and RIPK1 siRNA (ON-TARGET SMART pool) were obtained from Dharmacon (Chicago, IL). Caspase-8 siRNA (5'GAGUCUGUGCCCCAAAUCAATT3') was purchased from Qiagen (Crawley, UK). siRNA transfections were carried out with Lipofectamine RNAiMAX transfection reagent (Invitrogen, Paisley, UK) according to manufacturer's instructions.

Western blotting

Western blotting was carried out as previously described (21). cIAP1, cIAP2 and caspase-8 antibodies were from Enzo (Exeter, UK). XIAP, caspase-3, SMAC, APAF-1, caspase-9 and cytochrome c antibodies were from Cell Signaling Technology (Danvers, MA). β -actin antibody was from Sigma (Missouri) and FLIP antibody from AdipoGen (San Diego, CA). Secondary antibodies were purchased from LI-COR Biosciences (Lincoln, NE). Images were captured using an Odyssey Imaging System (LICOR, Lincoln, NE) at 12 bit dynamic range. Quantification of protein expression amounts was conducted as described previously (21).

Immunoprecipitation

Cells were pre-treated with 10 μ M z-VAD-fmk for 1 h prior to treatment with chemotherapy/TNF α /TL32711 combinations. Cells were lysed in CHAPS buffer (30 mM Tris pH7.5, 150 mM NaCl, 1% CHAPS). 1 μ g of caspase-8 p18 or IgG isotype control antibody (Santa Cruz, CA) was conjugated with 25 μ L ProteinG Dynabeads (Invitrogen,

Paisley, UK). Protein lysate (750 µg) was immunoprecipitated for 6 h at 4°C. Ripoptosome formation was analysed by Western blotting for RIPK1 (BD Transduction Laboratories).

Flow cytometry

Apoptosis induction was determined by Annexin V/propidium iodide analysis. Cells were harvested and stained according to the manufacturer's instructions (BD Biosciences, Oxford, UK). For measurements of mitochondrial membrane potentials, cells were incubated with 25 nM tetra-methyl-rhodamine ethyl ester (TMRE; Sigma, Missouri) for 15 minutes at 37°C. Cells were then trypsinized, washed in PBS and analyzed immediately. For FRET-based measurements of caspase-8 activation, Bax/Bak deficient HCT116 cells stably expressing the IETD FRET probe were generated and analyzed as described before (18).

Time lapse imaging and FRET analysis

Imaging settings and image analysis workflows for FRET disruption kinetics and for the timing of mitochondrial depolarisation at the single-cell level were described previously (17,38). All measurements were performed using stably transfected and clonally expanded cells. Cells were not synchronised prior to analysis to avoid potential cell cycle-dependent bias. Treatment durations exceeded two cell cycle durations to obtain authentic data from otherwise unperturbed cell populations.

Xenograft Experiments

Female BALB/c nude mice were maintained as previously described (39). All procedures were carried out in accordance with the Animals (Scientific Procedures) Act, 1986 under project licence (PPL 2590b). Mice were implanted in each flank with 2×10^6 HCT116 or 2.5×10^6 LoVo cells in Matrigel (BD, Oxford, UK). Upon establishment of $\sim 100 \text{ mm}^3$ tumours (HCT116, day 5; LoVo, day 11), mice were randomised to treatment groups. Groups were treated with vehicle, 5-FU/oxaliplatin, TL32711, or 5-FU/oxaliplatin in combination with TL32711. All treatments were administered by IP injection. TL32711 powder was reconstituted in 1% DMSO/Peanut oil (Sigma, Missouri), and mice were injected with 30 mg/kg three times per week. 5-FU was administered at 15 mg/kg in PBS (Gibco) on a 5 day on/2 day off schedule. Oxaliplatin was administered at 2 mg/kg in H₂O once a week. Tumour volume was assessed through measuring two dimensions using digital callipers three times per week. Two xenografts were collected per cell line from control mice to determine *in vivo* protein expression amounts.

Mathematical modelling

MATLAB including Statistics Toolbox Release 2014b (The MathWorks., Cambridge, UK) was used for mathematically modelling apoptosis signalling in response to chemotherapy, TL32711 or the combination of both. For processes subsequent to MOMP, we employed APOPTO-CELL, an ordinary differential equations-based model previously validated to reliably simulate apoptosis execution (21,40). This model provides kinetics of CFP-DEVD-YFP FRET substrate cleavage as an output that can be compared to experiments in which such probes are used. To simulate the slow and modest substrate cleavage prior to MOMP (“pre-MOMP ramps”), the upstream signalling was modelled using a heuristic function that feeds into and triggers the execution phase model. The technical implementation is described in Supplemental Information **SI1**.

Correlation of model predictions and drug effects on tumour growth

Tumour growth inhibitory effects (K_D) induced by the respective treatments were estimated from the *in vivo* tumour growth data. For this, we expressed the observed volume change over time ($\frac{dV}{dt}$) from the difference between tumour growth when untreated and a treatment-mediated reduction in growth (25,26). Model-predicted cell death and drug effects on *in vivo* tumour growth (K_D) were then tested for correlation (Pearson and Spearman). The technical implementation is described in Supplemental Information **SI1**.

Statistics

All statistical analyses were performed in Graphpad Prism (GraphPad Software, Inc, CA, USA). Data are shown as mean values \pm s.d., unless otherwise indicated. Two-tailed Student’s t tests were used for group comparisons. p values ≤ 0.05 were considered to be statistically significant.

Conflict of interest: The authors declare no conflict of interest.

Acknowledgements: The authors kindly acknowledge support for their work by grants from the European Union (FP7 APO-DECIDE) and Science Foundation Ireland/Department for Employment and Learning Northern Ireland Investigator Programme (14/IA/2582; 13/IA/1881). CTH and FAL received support from the Irish Research Council (GOIPD/2013/102; GOIPG/2014/1299). MR receives further support from the German Research Foundation (FOR2036, MO 3226/1-1).

References

1. de Gramont, A., Figer, A., Seymour, M., Homerin, M., Hmissi, A., Cassidy, J., Boni, C., Cortes-Funes, H., Cervantes, A., Freyer, G., Papamichael, D., Le Bail, N., Louvet, C., Hendler, D., de Braud, F., Wilson, C., Morvan, F., and Bonetti, A. (2000) Leucovorin and fluorouracil with or without oxaliplatin as first-line treatment in advanced colorectal cancer. *J Clin Oncol* **18**, 2938-2947
2. De Roock, W., De Vriendt, V., Normanno, N., Ciardiello, F., and Tejpar, S. (2011) KRAS, BRAF, PIK3CA, and PTEN mutations: implications for targeted therapies in metastatic colorectal cancer. *Lancet Oncol* **12**, 594-603
3. Hurwitz, H. I., Tebbutt, N. C., Kabbinavar, F., Giantonio, B. J., Guan, Z. Z., Mitchell, L., Waterkamp, D., and Tabernero, J. (2013) Efficacy and safety of bevacizumab in metastatic colorectal cancer: pooled analysis from seven randomized controlled trials. *Oncologist* **18**, 1004-1012
4. Hanahan, D., and Weinberg, R. A. (2011) Hallmarks of cancer: the next generation. *Cell* **144**, 646-674
5. Delbridge, A. R., Grabow, S., Strasser, A., and Vaux, D. L. (2016) Thirty years of BCL-2: translating cell death discoveries into novel cancer therapies. *Nat Rev Cancer* **16**, 99-109
6. Fulda, S. (2015) Promises and Challenges of Smac Mimetics as Cancer Therapeutics. *Clin Cancer Res* **21**, 5030-5036
7. Senzer, N. N., LoRusso, P., Martin, L. P., Schilder, R. J., Amaravadi, R. K., Papadopoulos, K. P., Segota, Z. E., Weng, D. E., Graham, M., and Adjei, A. A. (2013) Phase II clinical activity and tolerability of the SMAC-mimetic birinapant (TL32711) plus irinotecan in irinotecan-relapsed/refractory metastatic colorectal cancer. *J Clin Oncol (Meeting Abstracts)* **31**, 3621
8. Fulda, S. (2014) Molecular pathways: targeting inhibitor of apoptosis proteins in cancer--from molecular mechanism to therapeutic application. *Clin Cancer Res* **20**, 289-295
9. Gyrð-Hansen, M., and Meier, P. (2010) IAPs: from caspase inhibitors to modulators of NF-kappaB, inflammation and cancer. *Nat Rev Cancer* **10**, 561-574
10. Hector, S., and Prehn, J. H. (2009) Apoptosis signaling proteins as prognostic biomarkers in colorectal cancer: a review. *Biochim Biophys Acta* **1795**, 117-129
11. Tamm, I., Kornblau, S. M., Segall, H., Krajewski, S., Welsh, K., Kitada, S., Scudiero, D. A., Tudor, G., Qui, Y. H., Monks, A., Andreeff, M., and Reed, J. C. (2000) Expression and prognostic significance of IAP-family genes in human cancers and myeloid leukemias. *Clin Cancer Res* **6**, 1796-1803
12. Obexer, P., and Ausserlechner, M. J. (2014) X-linked inhibitor of apoptosis protein - a critical death resistance regulator and therapeutic target for personalized cancer therapy. *Frontiers in oncology* **4**, 197
13. Varfolomeev, E., Blankenship, J. W., Wayson, S. M., Fedorova, A. V., Kayagaki, N., Garg, P., Zobel, K., Dynek, J. N., Elliott, L. O., Wallweber, H. J., Flygare, J. A., Fairbrother, W. J., Deshayes, K., Dixit, V. M., and Vucic, D. (2007) IAP antagonists induce autoubiquitination of c-IAPs, NF-kappaB activation, and TNFalpha-dependent apoptosis. *Cell* **131**, 669-681
14. Vince, J. E., Wong, W. W., Khan, N., Feltham, R., Chau, D., Ahmed, A. U., Benetatos, C. A., Chunduru, S. K., Condon, S. M., McKinlay, M., Brink, R., Leverkus, M., Tergaonkar, V., Schneider, P., Callus, B. A., Koentgen, F., Vaux, D. L., and Silke, J. (2007) IAP antagonists target cIAP1 to induce TNFalpha-dependent apoptosis. *Cell* **131**, 682-693
15. Allensworth, J. L., Sauer, S. J., Lyster, H. K., Morse, M. A., and Devi, G. R. (2013) Smac mimetic Birinapant induces apoptosis and enhances TRAIL potency in inflammatory breast cancer cells in an IAP-dependent and TNF-alpha-independent mechanism. *Breast Cancer Res Treat* **137**, 359-371
16. Tenev, T., Bianchi, K., Darding, M., Broemer, M., Langlais, C., Wallberg, F., Zachariou, A., Lopez, J., MacFarlane, M., Cain, K., and Meier, P. (2011) The Ripoptosome, a signaling platform that assembles in response to genotoxic stress and loss of IAPs. *Mol Cell* **43**, 432-448

17. Hellwig, C. T., Kohler, B. F., Lehtivarjo, A. K., Dussmann, H., Courtney, M. J., Prehn, J. H., and Rehm, M. (2008) Real time analysis of tumor necrosis factor-related apoptosis-inducing ligand/cycloheximide-induced caspase activities during apoptosis initiation. *J Biol Chem* **283**, 21676-21685
18. Laussmann, M. A., Passante, E., Dussmann, H., Rauen, J. A., Wurstle, M. L., Delgado, M. E., Devocelle, M., Prehn, J. H., and Rehm, M. (2011) Proteasome inhibition can induce an autophagy-dependent apical activation of caspase-8. *Cell Death Differ* **18**, 1584-1597
19. Wang, C., and Youle, R. J. (2012) Predominant requirement of Bax for apoptosis in HCT116 cells is determined by Mcl-1's inhibitory effect on Bak. *Oncogene* **31**, 3177-3189
20. Rehm, M., Dussmann, H., Janicke, R. U., Tavaré, J. M., Kogel, D., and Prehn, J. H. (2002) Single-cell fluorescence resonance energy transfer analysis demonstrates that caspase activation during apoptosis is a rapid process. Role of caspase-3. *J Biol Chem* **277**, 24506-24514
21. Rehm, M., Huber, H. J., Dussmann, H., and Prehn, J. H. (2006) Systems analysis of effector caspase activation and its control by X-linked inhibitor of apoptosis protein. *The EMBO journal* **25**, 4338-4349
22. Schmid, J., Dussmann, H., Boukes, G. J., Flanagan, L., Lindner, A. U., O'Connor, C. L., Rehm, M., Prehn, J. H., and Huber, H. J. (2012) Systems Analysis of Cancer Cell Heterogeneity in Caspase-dependent Apoptosis Subsequent to Mitochondrial Outer Membrane Permeabilization. *J Biol Chem* **287**, 41546-41559
23. Dussmann, H., Rehm, M., Kogel, D., and Prehn, J. H. (2003) Outer mitochondrial membrane permeabilization during apoptosis triggers caspase-independent mitochondrial and caspase-dependent plasma membrane potential depolarization: a single-cell analysis. *J Cell Sci* **116**, 525-536.
24. Albeck, J. G., Burke, J. M., Aldridge, B. B., Zhang, M., Lauffenburger, D. A., and Sorger, P. K. (2008) Quantitative analysis of pathways controlling extrinsic apoptosis in single cells. *Mol Cell* **30**, 11-25
25. Benzekry, S., Lamont, C., Beheshti, A., Tracz, A., Ebos, J. M., Hlatky, L., and Hahnfeldt, P. (2014) Classical mathematical models for description and prediction of experimental tumor growth. *PLoS Comput Biol* **10**, e1003800
26. Simeoni, M., Magni, P., Cammia, C., De Nicolao, G., Croci, V., Pesenti, E., Germani, M., Poggesi, I., and Rocchetti, M. (2004) Predictive pharmacokinetic-pharmacodynamic modeling of tumor growth kinetics in xenograft models after administration of anticancer agents. *Cancer Res* **64**, 1094-1101
27. Van Schaeybroeck, S., Allen, W. L., Turkington, R. C., and Johnston, P. G. (2011) Implementing prognostic and predictive biomarkers in CRC clinical trials. *Nat Rev Clin Oncol* **8**, 222-232
28. Mitsuuchi, Y., Benetatos, C. A., Deng, Y., Haimowitz, T., Beck, S. C., Arnone, M. R., Kapoor, G. S., Seipel, M. E., Chunduru, S. K., McKinlay, M. A., Begley, C. G., and Condon, S. M. (2017) Bivalent IAP antagonists, but not monovalent IAP antagonists, inhibit TNF-mediated NF-kappaB signaling by degrading TRAF2-associated cIAP1 in cancer cells. *Cell death discovery* **3**, 16046
29. Sun, H., Nikolovska-Coleska, Z., Lu, J., Meagher, J. L., Yang, C. Y., Qiu, S., Tomita, Y., Ueda, Y., Jiang, S., Krajewski, K., Roller, P. P., Stuckey, J. A., and Wang, S. (2007) Design, synthesis, and characterization of a potent, nonpeptide, cell-permeable, bivalent Smac mimetic that concurrently targets both the BIR2 and BIR3 domains in XIAP. *Journal of the American Chemical Society* **129**, 15279-15294
30. Feoktistova, M., Geserick, P., Kellert, B., Dimitrova, D. P., Langlais, C., Hupe, M., Cain, K., Macfarlane, M., Hacker, G., and Leverkus, M. (2011) cIAPs Block Ripoptosome Formation, a RIP1/Caspase-8 Containing Intracellular Cell Death Complex Differentially Regulated by cFLIP Isoforms. *Mol Cell*
31. Tenev, T., Bianchi, K., Darding, M., Broemer, M., Langlais, C., Wallberg, F., Zachariou, A., Lopez, J., Macfarlane, M., Cain, K., and Meier, P. (2011) The Ripoptosome, a Signaling Platform that Assembles in Response to Genotoxic Stress and Loss of IAPs. *Mol Cell*

32. Clarke, P. R., and Allan, L. A. (2009) Cell-cycle control in the face of damage--a matter of life or death. *Trends in cell biology* **19**, 89-98
33. Vetma, V., Rozanc, J., Charles, E. M., Hellwig, C. T., Alexopoulos, L. G., and Rehm, M. (2017) Examining the In-Vitro Efficacy of the IAP Antagonist Birinapant as a Single-Agent or in Combination with Dacarbazine to Induce Melanoma Cell Death. *Oncology research*
34. Krepler, C., Chunduru, S. K., Halloran, M. B., He, X., Xiao, M., Vultur, A., Villanueva, J., Mitsuuchi, Y., Neiman, E. M., Benetatos, C., Nathanson, K. L., Amaravadi, R. K., Pehamberger, H., McKinlay, M., and Herlyn, M. (2013) The novel SMAC mimetic birinapant exhibits potent activity against human melanoma cells. *Clin Cancer Res* **19**, 1784-1794
35. Salvucci, M., Wurstle, M. L., Morgan, C., Curry, S., Cremona, M., Lindner, A. U., Bacon, O., Resler, A. J., Murphy, A. C., O'Byrne, R., Flanagan, L., Dasgupta, S., Rice, N., Pilati, C., Zink, E., Scholler, L. M., Toomey, S., Lawler, M., Johnston, P. G., Wilson, R., Camilleri-Broet, S., Salto-Tellez, M., McNamara, D. A., Kay, E. W., Laurent-Puig, P., Van Schaeybroeck, S., Hennessy, B. T., Longley, D. B., Rehm, M., and Prehn, J. H. (2017) A Stepwise Integrated Approach to Personalized Risk Predictions in Stage III Colorectal Cancer. *Clin Cancer Res* **23**, 1200-1212
36. Eissing, T., Kuepfer, L., Becker, C., Block, M., Coboeken, K., Gaub, T., Goerlitz, L., Jaeger, J., Loosen, R., Ludewig, B., Meyer, M., Niederal, C., Sevestre, M., Siegmund, H. U., Solodenko, J., Thelen, K., Telle, U., Weiss, W., Wendl, T., Willmann, S., and Lippert, J. (2011) A computational systems biology software platform for multiscale modeling and simulation: integrating whole-body physiology, disease biology, and molecular reaction networks. *Front Physiol* **2**, 4
37. Altrock, P. M., Liu, L. L., and Michor, F. (2015) The mathematics of cancer: integrating quantitative models. *Nat Rev Cancer* **15**, 730-745
38. Rehm, M., Parsons, M. J., and Bouchier-Hayes, L. (2015) Measuring caspase activity by Forster resonance energy transfer. *Cold Spring Harbor protocols* **2015**, pdb prot082560
39. Wilson, T. R., McLaughlin, K. M., McEwan, M., Sakai, H., Rogers, K. M., Redmond, K. M., Johnston, P. G., and Longley, D. B. (2007) c-FLIP: a key regulator of colorectal cancer cell death. *Cancer Res* **67**, 5754-5762
40. Huber, H. J., Rehm, M., Plchut, M., Dussmann, H., and Prehn, J. H. (2007) APOPTO-CELL--a simulation tool and interactive database for analyzing cellular susceptibility to apoptosis. *Bioinformatics* **23**, 648-650

Figure Legends

Figure 1: XIAP depletion and IAP antagonist TL32711 sensitize CRC cell lines to chemotherapy-induced cell death. (A) AnnexinV/PI staining of HCT116 and HCT116 xiap⁻⁰ cells treated with 5FU (10 μ M) and oxaliplatin (2 μ M) for up to 48 h. (B) AnnexinV/PI staining of HCT116 and HCT116 xiap⁻⁰ cells treated with oxaliplatin and 5FU for up to 48 h in presence or absence of 20 μ M pan-caspase inhibitor z-VAD-fmk. (C,D) Annexin V/PI staining of HCT116 and LoVo cells 48 h following single or combination treatment with 10 μ M 5FU, 2 μ M oxaliplatin and 1 μ M TL32711. All data are shown as mean \pm s.e.m. from n = 3 independent experiments.

Figure 2: IAP antagonist TL32711 promotes cIAP1,2 depletion, formation of complex II and caspase-8/RIPK1-dependent cell death. (A) Western blot analysis of cIAP1, cIAP2 and XIAP expression in HCT116 and LoVo cells following treatment with 1 μ M TL32711. β -actin served as loading control. (B) Western blot analysis of cIAP1, cIAP2 and XIAP 24 h following treatment with varying concentrations of TL32711 in HCT116 and LoVo cells. β -actin served as loading control. (C) Western blot analysis of RIPK1 and procaspase-8 following caspase-8 immunoprecipitation 48 h following treatment with 10 μ M 5FU, 2 μ M oxaliplatin and 3 h after addition of 1 μ M TL32711 in the presence of 10 μ M z-VAD-fmk in HCT116 cells. Input controls demonstrate presence of RIPK1 and procaspase-8 in all lysates. (D) Caspase-8-like (IETDase) activity was measured in HCT116 (Bax/Bak)^{-/-} cells expressing a CFP-IETD-YFP FRET probe and that were transfected with scrambled control (SCR) siRNA or siRNA targeting procaspase-8 (C8si). Data are shown as mean \pm s.d. from triplicates. Experiment was repeated twice with similar results. (E) Mitochondrial depolarisation as determined by loss of TMRE uptake in HCT116 cells transfected with scrambled control (SCR) siRNA or siRNA targeting procaspase-8 (C8si). Cells were (co-)treated with 1 μ M TL32711 (TL), 10 μ M 5FU and 2 μ M oxaliplatin (oxali) for 48 h. Western blot insert demonstrates efficient depletion of procaspase-8 (PC8) expression. (F) Annexin V/PI staining of HCT116 transfected with scramble control (SCR) siRNA or siRNA targeting RIPK1 and (co-)treated with 1 μ M TL32711 (TL), 10 μ M 5FU and 2 μ M oxaliplatin (oxali) for 48 h. Western blot insert demonstrates efficient depletion of RIPK1 expression. *p < 0.05; **p < 0.01.

Figure 3: Single-cell real-time imaging identifies two distinct caspase activation patterns leading to apoptosis execution in TL32711-based combination treatments. (A) Pseudo

coloured CFP/YFP emission ratio images of a group of HCT-116 cells expressing a DEVDase FRET probe treated with 5FU/oxaliplatin (10 μ M/ 2 μ M) in combination with TL32711 (1 μ M). DEVDase activity resulted in FRET probe cleavage and displayed as an increase in the CFP/YFP emission ratio. Loss of TMRM fluorescence indicates mitochondrial depolarisation as a consequence of MOMP. Time stamps indicate time after stimulus addition. **(B)** Exemplary DEVDase response profiles of HCT116 cells (upper panels) treated with 5FU/oxaliplatin, TL32711 or the combination of both. Cells responding to 5FU/oxaliplatin predominantly showed late DEVDase activity, subsequent to the onset of mitochondrial depolarisation and corresponding to the canonical activation of the intrinsic apoptosis pathway **(i)**. Cells responding to TL32711 single treatment exclusively displayed response patterns resembling the one shown in **(ii)**, with mild DEVDase activity converted into rapid substrate cleavage following onset of mitochondrial depolarisation. Cells treated with the combination of 5FU/oxaliplatin and TL32711 frequently presented substrate cleavage ramps prior to the onset of mitochondrial depolarisation **(iii)**, as well as response patterns without pre-MOMP caspase activity, resembling those shown in **(i)**. Similar response characteristics were observed in LoVo cells **(i-iii)**. **(C)** Quantification of response types and kinetics. For all HCT116 and LoVo cells responding to the treatments, the response characteristics were analysed and quantified. Parameters evaluated included the onset time of pre-MOMP caspase activity (time from drug addition to initiator caspase activation), the slope of pre-MOMP substrate cleavage as a measure of caspase activity, the mitochondrial MOMP threshold (amount of substrate cleaved at the time MOMP-induced mitochondrial depolarisation begins), as well as the onset time of the execution phase. Data are shown median +/- quartiles.

Figure 4: Mathematical simulations of apoptosis signalling can recapitulate death profiles and apoptosis sensitization by IAP antagonist TL32711. **(A)** Overview of the architecture of the developed model. Data from experimental analyses of signalling kinetics upstream of MOMP were used to construct mathematical functions replicating early signalling characteristics. These then feed into and trigger the execution phase of apoptosis. The execution phase was simulated using a validated model based on coupled ordinary differential equations. The primary model output reflecting cellular apoptosis competency is the calculated amount of cellular substrates cleaved by caspases. A substrate cleavage above 25% is considered to be sufficient for successful apoptosis execution. The diagram insert shows exemplary cell behaviours, such as non-responsive cells and cells responding at

different times and with different SC thresholds for MOMP induction. See methods section for details. **(B)** Mean expression of key players of apoptosis execution as quantified in HCT116 and LoVo cells from $n = 3$ experiments using quantitative immunoblotting. **(C)** Cellular protein expression converted into normal distributions. Random sampling from these distributions served to parameterise the apoptosis execution module of the mathematical model. **(D,E)** The behaviour of ensembles of 1,000 cells per treatment condition was mathematically modelled for HCT116 cells **(D)** or LoVo cells **(E)**. Cell ensembles were parameterised as described in the methods and results sections. Each line represents the behaviour of one cell in the modelled ensemble. Near-vertical lines indicate phases of rapid substrate cleavage as observed during apoptosis execution. Ramps represent phases of pre-MOMP substrate cleavage. Modelling results replicate experimental findings: Cells heterogeneously respond with apoptosis induction and execution, with combination treatment of chemotherapy and TL32711 causing higher amounts of cell death.

Figure 5: Systems modelling predicts increased apoptosis resistance of xenografted HCT116 and LoVo cell tumours, which can be overcome by chemotherapy/TL32711 co-treatment. **(A)** Comparison of baseline protein expression between *in vitro* and *in vivo* (day 7 after inoculation) growth conditions prior to treatment. For the *in vivo* setting, two xenografts were collected per cell line. Representative immunoblots from whole cell extracts of HCT116 and LoVo cells are shown. **(B, C)** For each cell line, protein expression amounts (nM) were quantified ($n = 3-4$ detections) using quantitative immunoblotting. **(D,E)** The apoptosis competency of ensembles of 1,000 cells per treatment condition was mathematically modelled for HCT116 cells **(D)** or LoVo cells **(E)** for *in vivo* growth conditions.

Figure 6: Mathematical modelling captures drug effects observed *in vivo* and predicts treatment responses. **(A,B)** Accumulated cell death as obtained from mathematically modelling apoptosis execution in HCT116 or LoVo cell ensembles at *in vivo* growth conditions. **(C,D)** Fold change in tumour volume in HCT116 and LoVo xenograft models in control, TL32711, 5FU and oxaliplatin and 5FU, oxaliplatin and TL32711 groups. Treatments of 15 mg/kg 5FU, 2 mg/kg oxaliplatin and 30 mg/kg TL32711 were administered by IP injection as indicated. Error bars indicate s.e.m. **(D)** Western blot analysis of cIAP1, cIAP2 and XIAP expression in HCT116 and LoVo xenograft tumours before and after treatment. β -actin served as loading control. **(E,F)** Pooled results from fitted tumour growth curves obtained from individual tumours. Traces indicate mean volume changes over time; shaded areas indicate variance (25th – 75th percentile), obtained by bootstrapping, within the

treatment group. **(G)** Correlation analysis between simulated cell death and the drug effects (K_D) obtained from (E, F). Error bars indicate s.d., obtained from bootstrapping.

Supplemental Figure 1: Mathematical simulations of *in vitro* and *in vivo* apoptosis competency subsequent to MOMP. **(A-D)** The behaviour of ensembles of 1,000 cells per treatment condition was mathematically modelled for HCT116 cells *in vitro* **(A)** and *in vivo* **(B)** or LoVo cells *in vitro* **(C)** and *in vivo* **(D)**. Cell ensembles were parameterised as described in the main manuscript. Each line represents the behaviour of one cell in the modelled ensemble. High amounts of substrate cleavage indicate that modelled cells are capable of executing apoptosis efficiently. Absent substrate cleavage or low amounts of substrate cleavage indicate failure to efficiently execute apoptosis. The simulation results indicate that post-MOMP heterogeneity is particularly prominent at *in vivo* conditions.

Fig.1

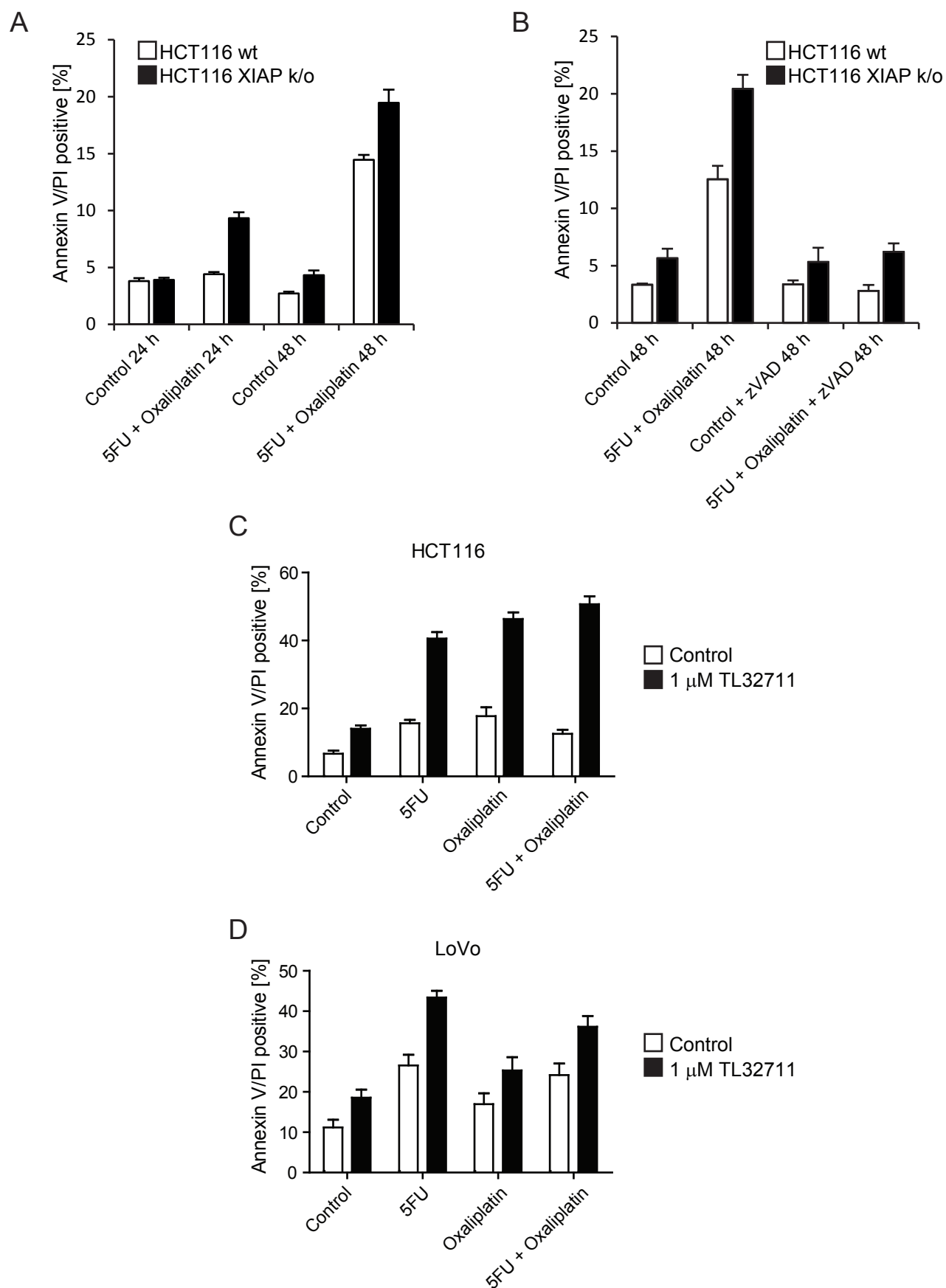
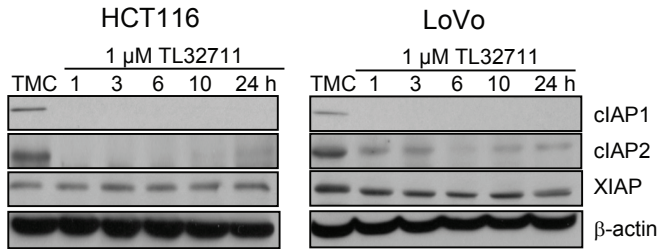
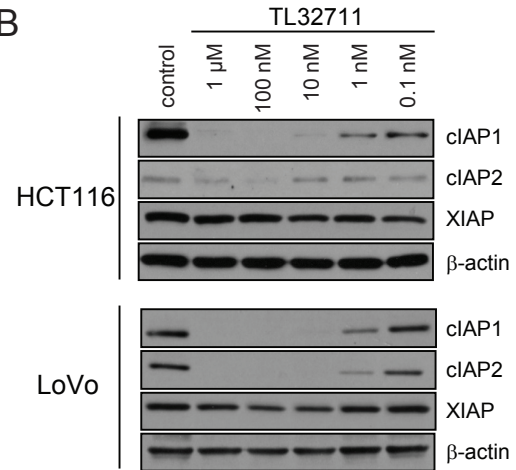


Fig.2

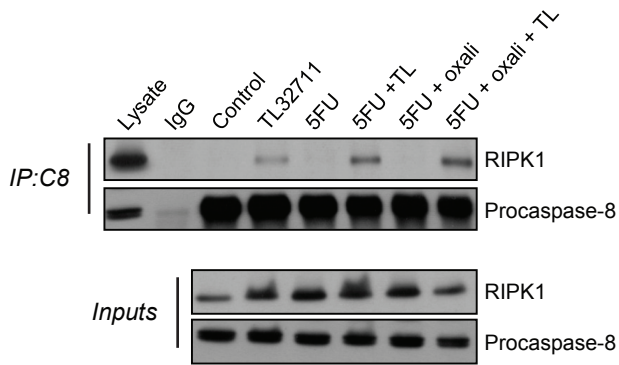
A



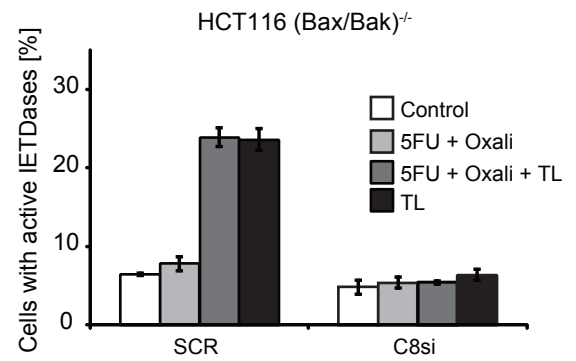
B



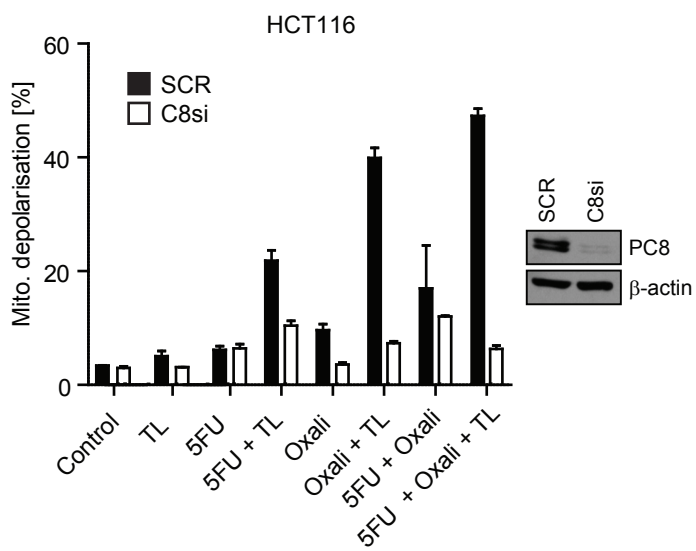
C



D



E



F

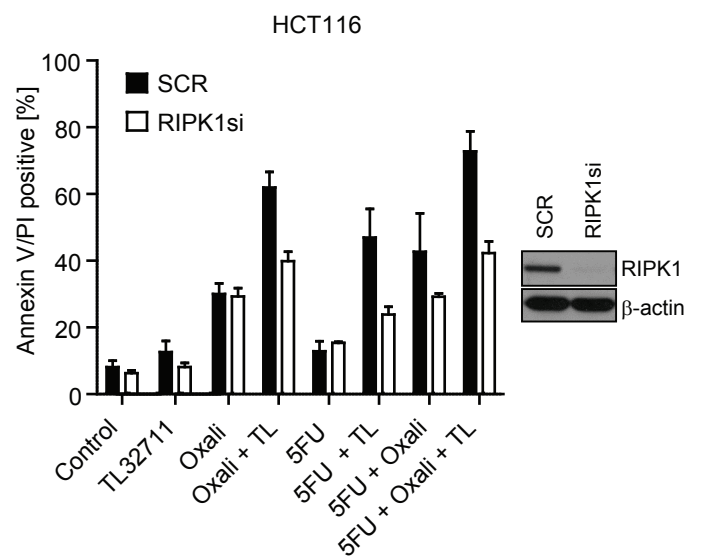


Fig.3

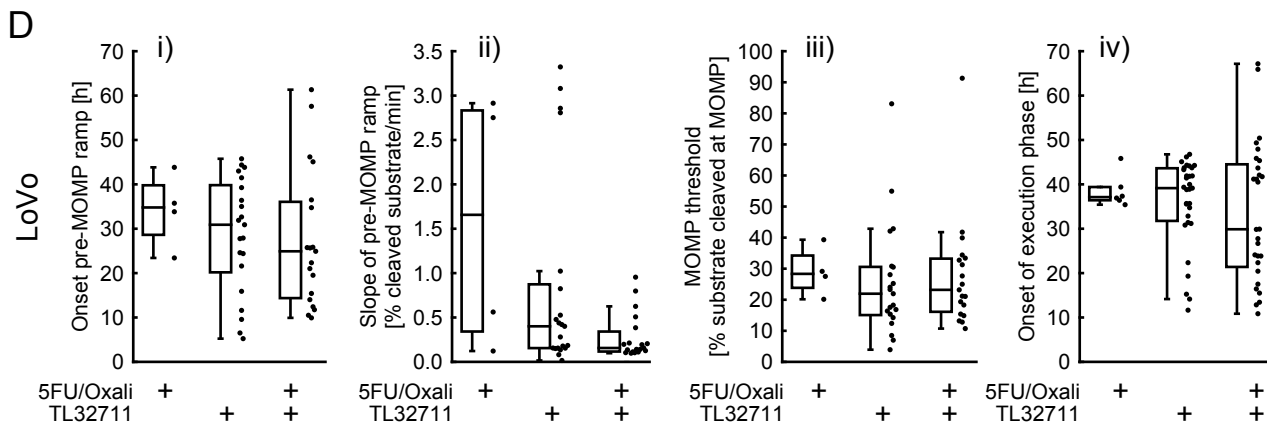
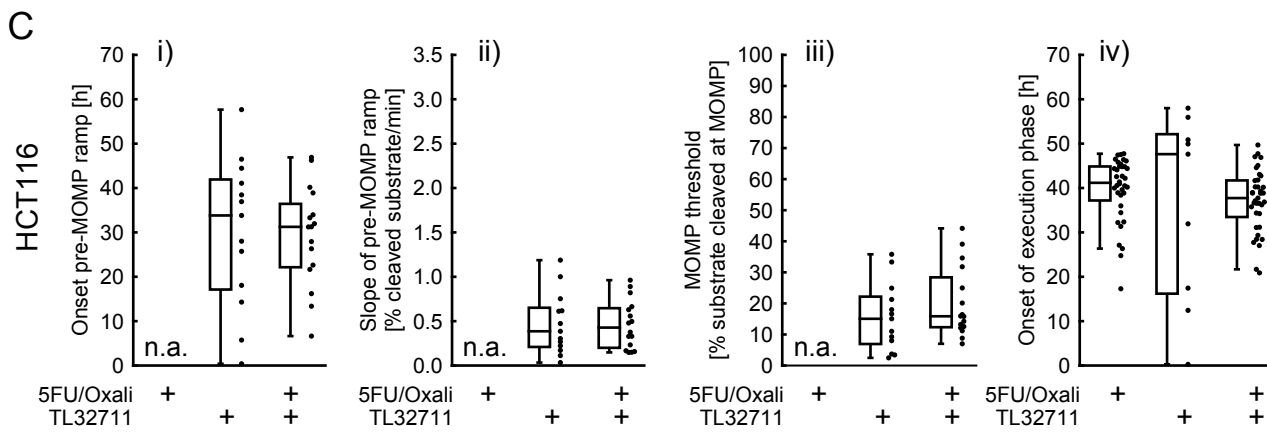
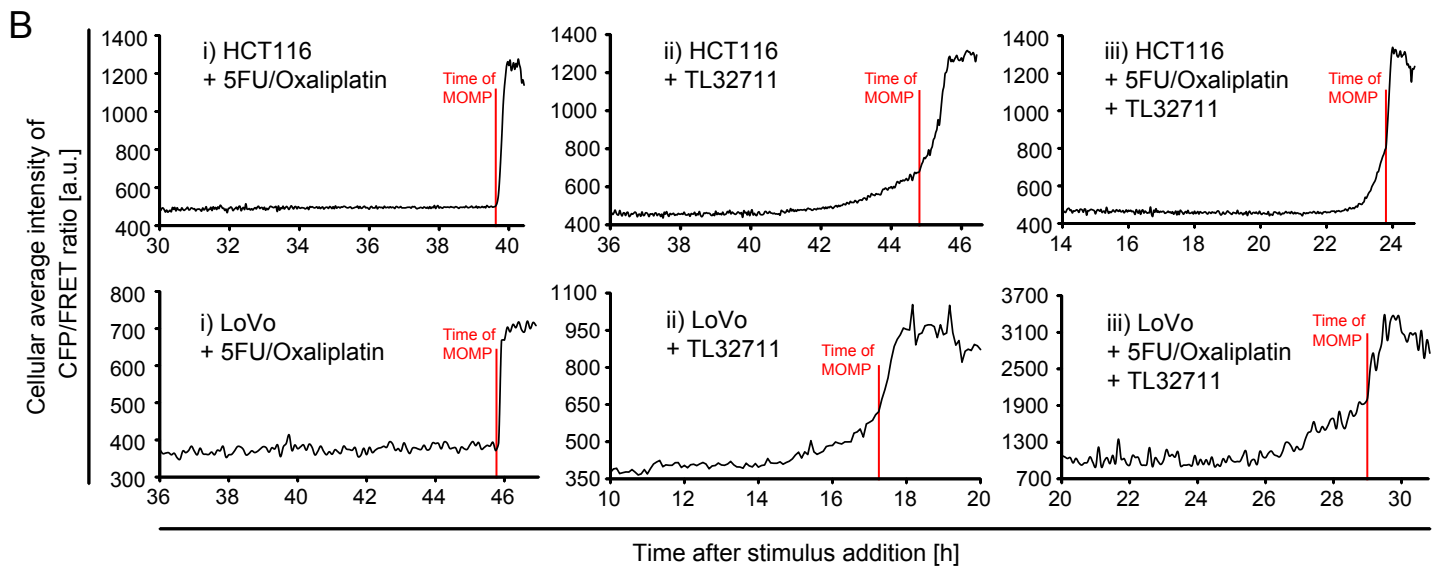
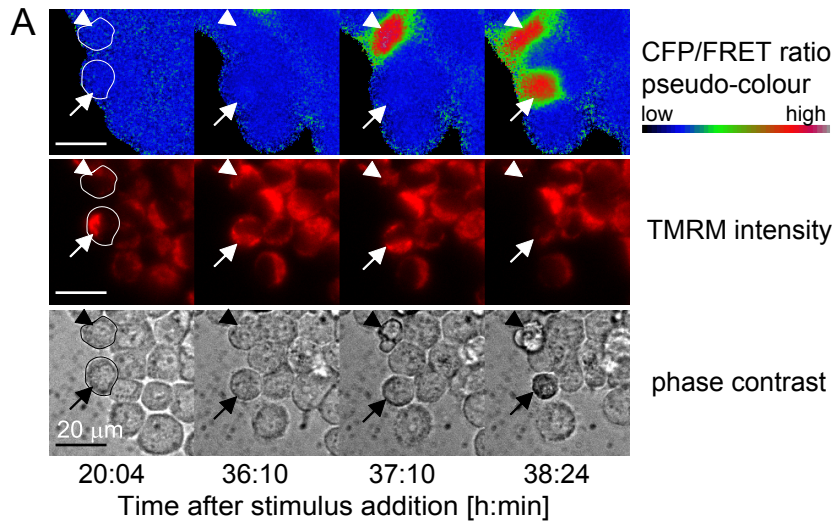


Fig.4

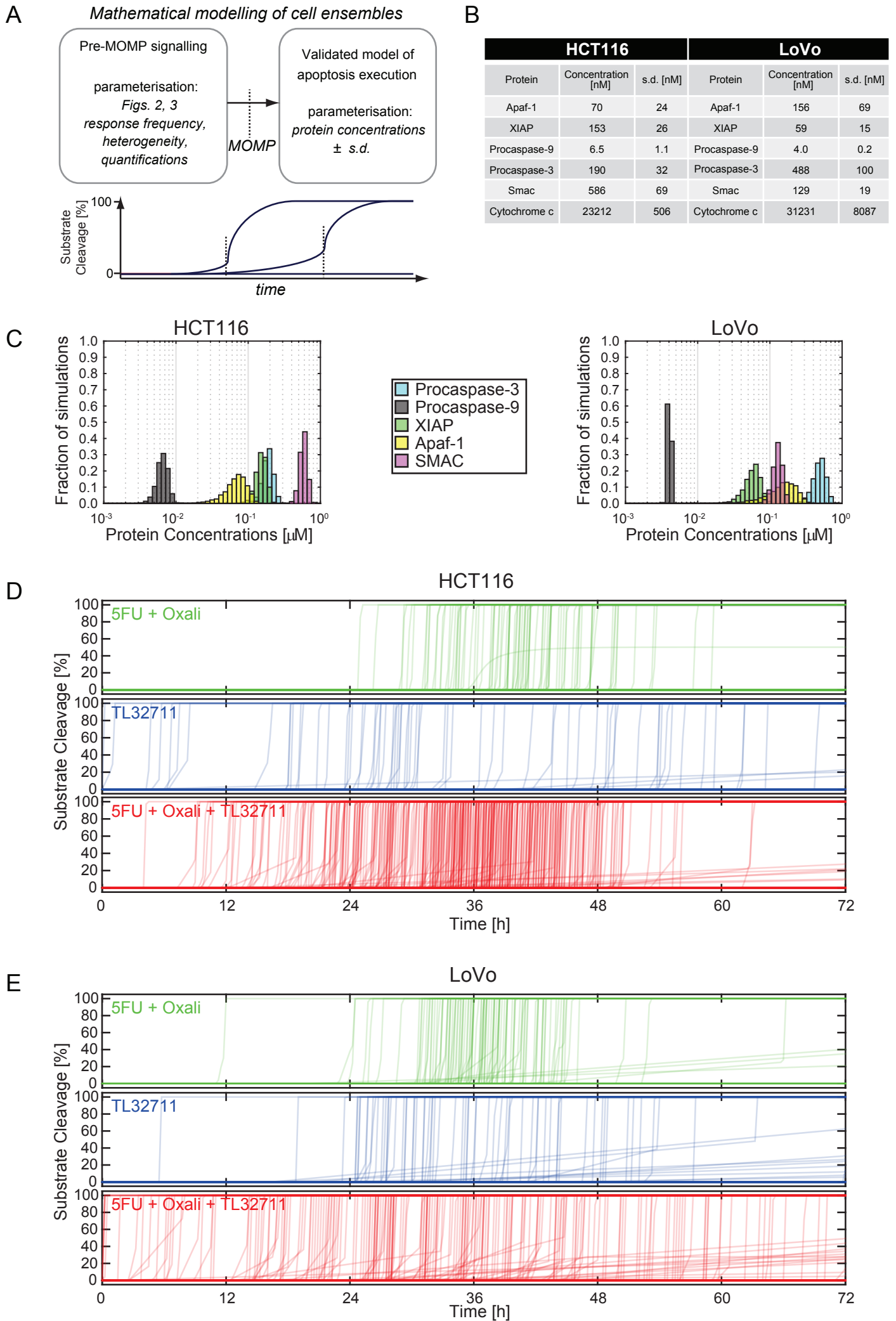


Fig.5

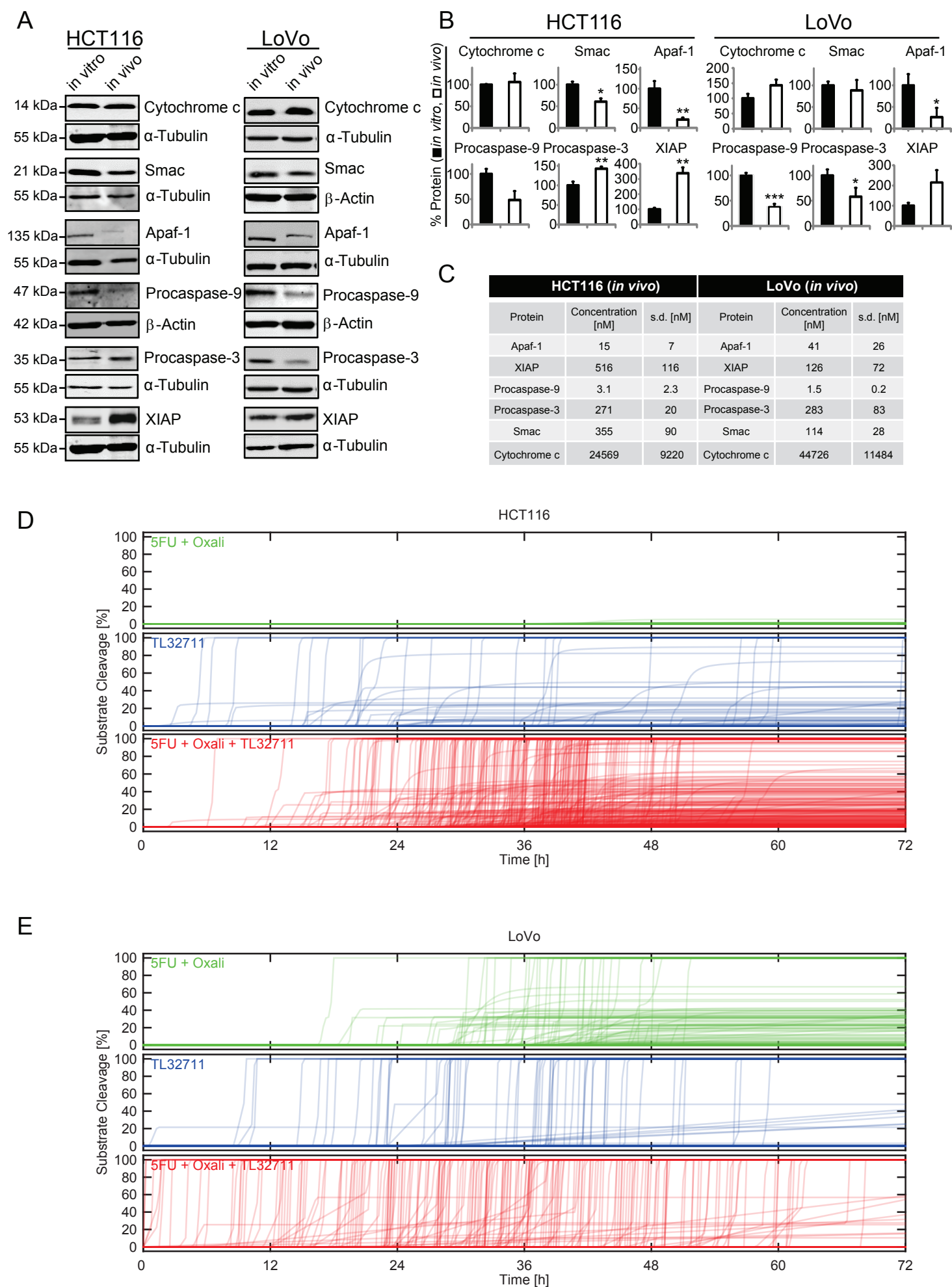
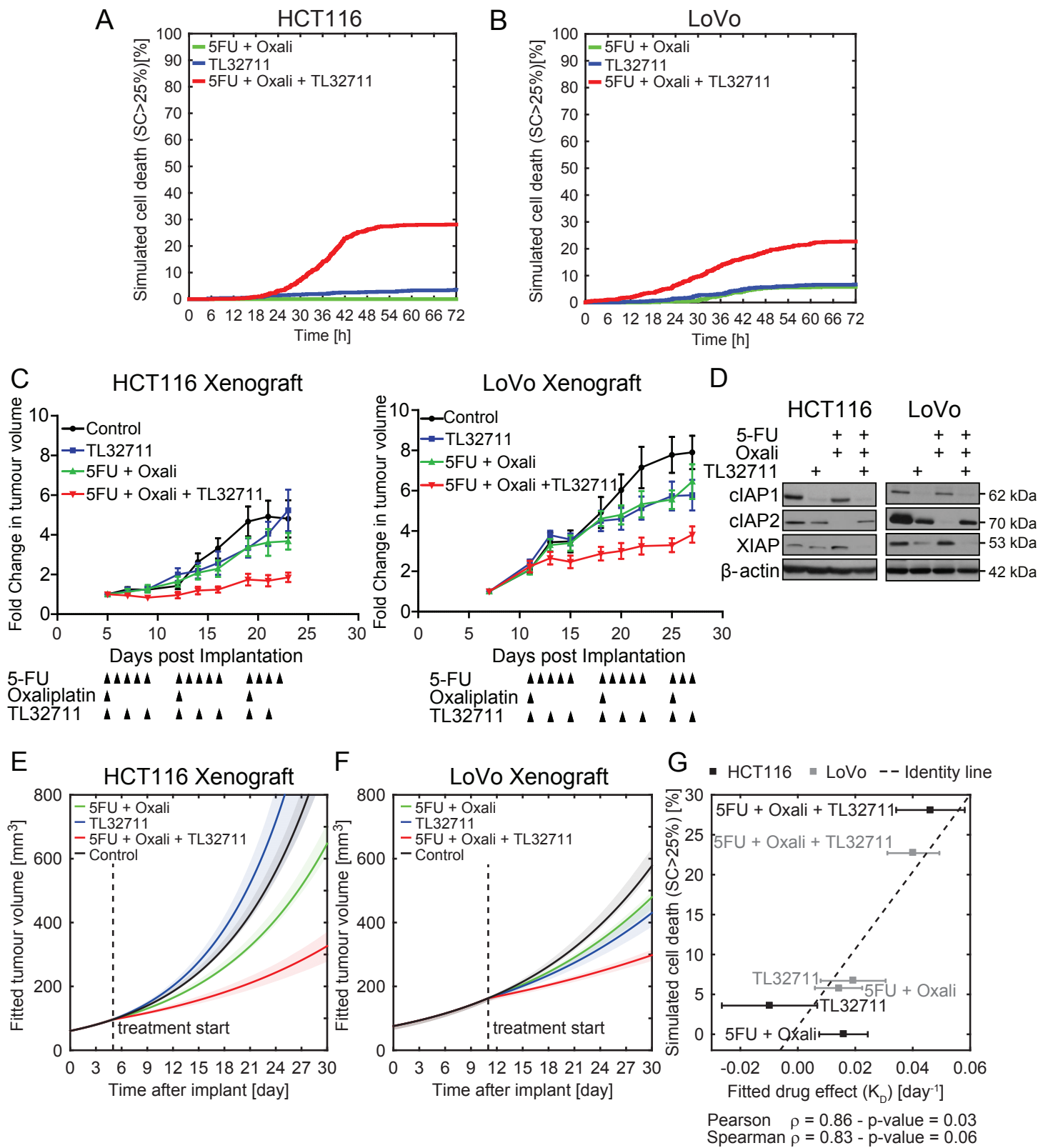


Fig.6



Technical implementation of mathematical models and predictions on drug effects on tumour growth.

Mathematical modelling

We used MATLAB equipped with the Statistics, Parallel Computing, and Optimization toolboxes (MATLAB, release 2014b, The MathWorks, Inc., Cambridge, UK) to build a mathematical model that simulates apoptosis signal transduction in response to chemotherapy, TL32711 or the combination of both in cell populations. To model the processes subsequent to mitochondrial outer membrane permeabilisation (MOMP) we employed APOPTO-CELL, an ordinary differential equations (ODE)-based model previously validated to reliably simulate signal transduction during the apoptosis execution phase (1, 2), as a module of the overall modelling framework. This model provides the kinetics of CFP-DEVD-YFP FRET substrate cleavage as an output, providing the possibility for comparison to experiments in which such probes are used. To simulate the slow and modest substrate cleavage prior to MOMP (“pre-MOMP ramps”), the upstream signalling was modelled using a heuristic function which feeds into and triggers the execution phase ODE model. This function captures both the period where FRET substrate is not yet cleaved as well as the period of on-going pre-MOMP substrate cleavage. Combined with the APOPTO-CELL model of the apoptosis execution phase, FRET substrate cleavage (SC) over time can thereby be described in its entirety:

$$SC(t) = \begin{cases} 0, & t_{start\ treatment} \leq t < t_{onset\ pre-MOMP\ ramp} \\ \frac{\Delta SC}{\Delta ramp\ time} t, & t_{onset\ pre-MOMP\ ramp} \leq t < t_{onset\ execution\ phase} \\ APOPTO - CELL(t, SC_{onset\ execution\ phase}, TL32711, \mathbf{P}), & t \geq t_{onset\ execution\ phase} \end{cases}$$

Here, $\frac{\Delta SC}{\Delta ramp\ time}$ denotes the slope of pre-MOMP substrate cleavage and $SC_{onset\ execution\ phase}$ the amount of substrate cleaved at the time the rapid execution phase is initiated, the latter being modelled by the default APOPTO-CELL module. The concentration of IAP-antagonists is accounted for by TL32711. The vector \mathbf{P} comprises protein expression amounts for Procaspase-3, Procaspase-9, SMAC, XIAP and Apaf-1 as further model inputs. Ranges for response times, frequencies and cleavage rates required for model parameterisation were obtained from experimental data collected from HCT116 and LoVo cell ensembles treated with 5-FU/Oxaliplatin, TL32711 or 5-FU/Oxaliplatin + TL32711. Protein expression ranges were obtained from quantitative analyses of HCT116 and LoVo cells grown *in vitro* or *in vivo* (Fig.4B, Fig.5C). From the input data we defined normal distributions by the measured means and standard deviations and applied bootstrapping to build ensembles of 1,000

cells for each treatment condition and cell line for both *in vitro* and *in vivo* scenarios. This allowed us to reflect the heterogeneity of large cell ensembles within the modelling framework and to simulate or predict the behaviour of cell populations in response to treatment *in vitro* and *in vivo*.

Correlation of model predictions and drug effects on tumour growth

Tumour growth inhibitory effects (K_D) induced by the respective treatments were estimated from the *in vivo* tumour growth data. For this, we expressed the observed volume change over time ($\frac{dV}{dt}$) from the difference between tumour growth when untreated and a treatment-mediated reduction in growth, with the latter being proportional to the tumour volume (3, 4):

$$\frac{dV}{dt} = \begin{cases} aV \left(1 - \frac{V}{K}\right), & t < t_{start\ treatment} \\ aV \left(1 - \frac{V}{K}\right) - K_D V, & t \geq t_{start\ treatment} \end{cases}$$

The tumour volume $V(t)$, when untreated, can be expressed as:

$$V(t) = \frac{KV_0}{V_0 + (K - V_0)e^{-at}}$$

where V_0 indicates the volume of the individual tumours at time of first measurement ($V(t = t_0)$). The parameters K and a are cell-line specific constants representing the “carrying capacity” (maximal asymptotic growth) and the proliferation rate, respectively. We fitted each volume measurement (days 5, 7, 9, 12, 14, 16, 19, 21, 23 and days 11, 13, 15, 18, 29, 22, 25, 27 for HCT116 and LoVo, respectively) using the MATLAB function *lsqcurvefit* with initial values for $V_0 = 25 [mm^3]$, $a = 0.2 [day^{-1}]$, $K = 300 [mm^3]$ and $K_{D_{Control}} = K_{D_{5FU + Oxali}} = K_{D_{TL32711}} = K_{D_{5FU + Oxali + TL32711}} = 0.01 [day^{-1}]$.

We computed the mean and s.d. of the bootstrapped K_D across 1000 iterations as a measure of experimental treatment efficacy. For each cell line and treatment, we computed the fraction of the simulated cell ensemble that was modelled to undergo apoptosis (SC>25% at 72 h), (**Fig.6A-B**). Model-predicted cell death and drug effects on *in vivo* tumour growth (mean bootstrapped K_D) were then tested for correlation (Pearson and Spearman), (**Fig.6G**).

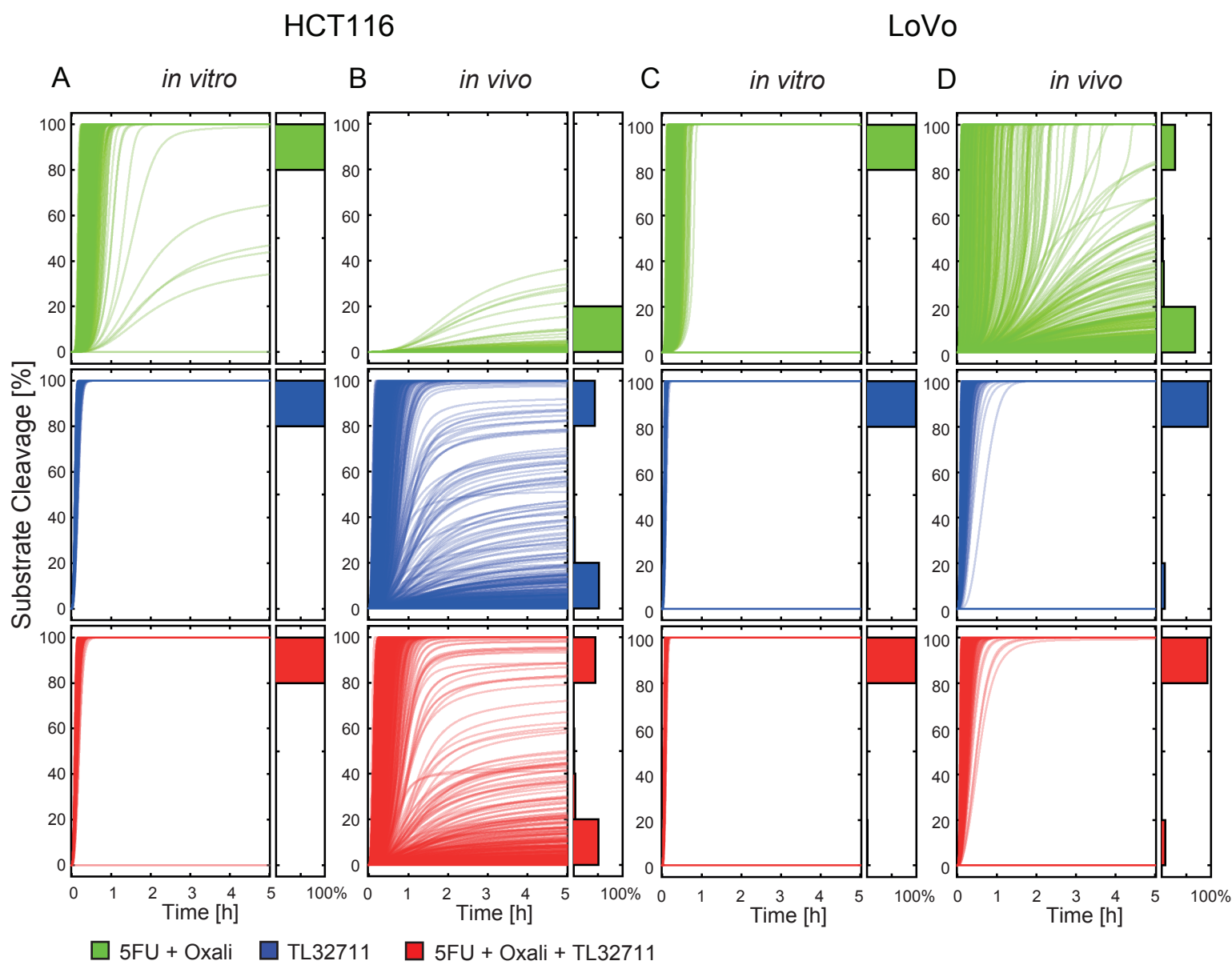
Modelling code and associated data are available as a Zenodo repository

(<https://doi.org/10.5281/zenodo.1067500>)

References

1. Huber HJ, Rehm M, Plchut M, Dussmann H, Prehn JH. APOPTO-CELL--a simulation tool and interactive database for analyzing cellular susceptibility to apoptosis. *Bioinformatics*. 2007 Mar 1;23(5):648-50.
2. Rehm M, Huber HJ, Dussmann H, Prehn JH. Systems analysis of effector caspase activation and its control by X-linked inhibitor of apoptosis protein. *Embo J*. 2006 Sep 20;25(18):4338-49.
3. Benzekry S, Lamont C, Beheshti A, Tracz A, Ebos JM, Hlatky L, et al. Classical mathematical models for description and prediction of experimental tumor growth. *PLoS Comput Biol*. 2014 Aug;10(8):e1003800.
4. Simeoni M, Magni P, Cammia C, De Nicolao G, Croci V, Pesenti E, et al. Predictive pharmacokinetic-pharmacodynamic modeling of tumor growth kinetics in xenograft models after administration of anticancer agents. *Cancer Res*. 2004 Feb 01;64(3):1094-101.

Sup. Fig. 1



Supplemental Figure 1: Mathematical simulations of *in vitro* and *in vivo* apoptosis competency subsequent to MOMP. (A-D) The behaviour of ensembles of 1,000 cells per treatment condition was mathematically modelled for HCT116 cells *in vitro* (A) and *in vivo* (B) or LoVo cells *in vitro* (C) and *in vivo* (D). Cell ensembles were parameterised as described in the main manuscript. Each line represents the behaviour of one cell in the modelled ensemble. High amounts of substrate cleavage indicate that modelled cells are capable of executing apoptosis efficiently. Absent substrate cleavage or low amounts of substrate cleavage indicate failure to efficiently execute apoptosis. The simulation results indicate that post-MOMP heterogeneity is particularly prominent at *in vivo* conditions.